Experimental investigation of the physical foaming of tannin-based thermoset foams

Z. Marie, V. Nicolas, A. Celzard, V. Fierro

Experimental investigation of the physical foaming of tannin-based thermoset foams

Z. Marie, V. Nicolas*, A. Celzard, V. Fierro

Université de Lorraine, CNRS, IJL, F-88000 Epinal, France

Abstract

The physical foaming of thermosetting biosourced formulations, mainly based on tannin extracts and furfuryl alcohol, was investigated in-depth with a specially designed setup. Mass loss, volume expansion, and temperature measured at the bottom, in the middle and at the top of foams were continuously monitored during their preparation, from the first moment after the liquid formulation was poured into a mould until the final foams hardened and dried. Correlations were found between the observed phenomena. Thus, successive foaming mechanisms involving: (i) phase change of the blowing agent at 55°C, (ii) pore opening at a critical inner pressure, which induced 4% mass loss, and (iii) surface evaporation, could be elucidated and were discussed. The effects of the amounts of blowing agent on the one hand, which increases foam expansion, and of polymerisation catalyst on the other hand, which reduces the induction time, were also investigated, leading to some shifts in the aforementioned phenomena. The present results are certainly relevant to other self-foaming formulations based on thermosetting polymers such as traditional polyurethanes expanded by physical foaming with pentane.

Keywords: Thermoset foams; Physical foaming; Tannin; Data acquisition; Heat and mass transfers; biosourced formulation

* Corresponding author. Tel: + 33 372 74 96 54. Fax: + 33 372 74 96 38. E-mail address : vincent.nicolas@univ-lorraine.fr (V. Nicolas)

1 Introduction

Rigid foams are mature products that are abundantly used in various sectors, such as construction, transport, and industry in general (Landrock, 1995). Among them, phenolic foams are of special interest because of their low cost, low density, good mechanical and insulating properties, and excellent retardance to fire associated with low smoke emission and no dripping of molten plastic (Denslow and Rickle, 1989; Haberstroh and Schlumm, 2011; Mendelsohn et al., 1979b, 1979a; Rangari et al., 2007; Shen and Nutt, 2003; Shutov, 1984). However, they are produced from toxic and non-renewable raw materials, hence the need of finding cheap, abundant, ecological but still effective substitutes.

Many trials were successfully carried out for replacing phenol by poorly or non-toxic natural phenolic molecules, either partly for instance by lignin (Carvalho et al., 2003), by cardanol (Bo et al., 2016, 2018) or by hydrolysable tannins (Lagel et al., 2014), or even completely by condensed tannins of various natures (Lacoste et al., 2013, 2014; Martinez de Yuso et al., 2014; Tondi et al., 2009a). The latter materials were the most promising ones, since many formulations were developed, leading to acid-free (Basso et al., 2014a), solvent-free (Basso et al., 2013a), and even formaldehyde-free (Basso et al., 2011, 2015) foams, all having relevant physical properties for most of the traditional uses of phenolic foams (packaging, cushioning, insulation, building materials, automobiles, aircrafts and marine structures, electronics and flame retardance).

Although continuous preparation processes have been suggested (Basso et al., 2014b), tannin-based foams are mainly produced in batch until now. The problem with such preparation method is the impact of the experimental conditions on the structure, and hence on the properties, of the resultant foam. Indeed, most tannin-based formulations are self-foaming, i.e., based on the heat induced by polymerisation reactions and by which gases are produced, thereby leading to a dramatic increase of volume. It is then easy to understand that,

for instance, changing the nature and/or the size of the mould for a given amount of formulation poured into it leads to different results since part of the heat is absorbed by the walls of the mould. Therefore, the higher is the contact area with the mould, and/or the higher is the thermal effusivity of the mould, the lower will be the temperature inside the foam and the lower will be its expansion. As a result, foams with higher density will be obtained, having smaller cells, higher mechanical properties but lower insulating character, and so forth (Letellier et al., 2017a).

In a similar way, introducing higher amounts of formulation in a given mould will produce more heat upon polymerisation, thus a higher expansion, larger cells, lower mechanical strength, etc. (Letellier et al., 2017a). Beyond a critical quantity of reagents, and whereas all proportions are kept constant, a potentially dangerous auto-acceleration of the polymerisation reactions (Trommsdorff effect) may even occur. For avoiding reconsidering completely the formulations each time some experimental conditions are changed (amounts of reactants, air temperature, moulds, etc.), less empiricism is thus necessary.

In the recent past, first attempts for streamlining the batch production of thermoset foams have been carried out and applied to polyurethane (Bikard et al., 2005, 2007; Bouayad et al., 2008, 2009; Ireka et al., 2015; Karimi and Marchisio, 2015) and tannin-based (Basso et al., 2013d, 2013b, 2013c) foams. In the latter case, a special commercial device initially developed for investigating the preparation of polyurethane foams, called FOAMAT® (Messtechnik, Germany), was used. The FOAMAT® 285 Foam Qualification System allows measuring at the same time the changes of several parameters during foam growth, such as temperature (at a fixed position), foam height, pressure exerted on the bottom of the mould, and dielectric polarisation (related to the extent of polymerisation reactions). With such system, temperature and expansion are the most commonly measured quantities, and are generally measured only at the beginning or until the three-quarters of the foaming process.

In the present work, further advances in the characterisation and in the understanding of the foaming process of thermosetting tannin-based formulations are proposed. After a foaming model was developed in a former paper (Marie et al., 2019), a new experimental setup is offered herein for the ultimate purpose of refining the mechanisms of expansion of such formulations, and better taking into account the effect of some ingredients on the final foams properties. Compared to previous experiments carried out with the FOAMAT®, the present system allows temperature measurements for very long times, i.e., including foam cooling, and at three different positions within the material instead of a single one. Additionally, the mass changes were measured continuously, which had never been done so far for this kind of formulations. Based on the corresponding results, and especially by examining the extent and the synchronisation of the observed changes, new information about foaming mechanisms and about the impact of selected ingredients could be obtained.

2 Materials and Methods

2.1. Preparation of tannin-based foams

In the present work, the formulation abundantly described elsewhere and referred to as the "standard" one for tannin-based foams (see for instance (Delgado-Sánchez et al., 2018a; Tondi et al., 2009a, 2009b; Zhao et al., 2010) and refs. therein) was used. It is based on mimosa tannin extract, commercially available under the name FINTAN-OP and kindly provided by the company SilvaChimica (St. Michele Mondovi, Italy). It typically comprises 80% of flavonoid compounds (i.e., condensed tannins of prorobinetinidin type (Braghiroli et al., 2012)), which are soluble in water and can easily react with both furfuryl alcohol and formaldehyde in order to lead to crosslinked phenolic-furanic resins (Basso et al., 2014b; Delgado-Sánchez et al., 2018b; Li et al., 2012a; Pizzi et al., 2008). The latter are prone to foam spontaneously as soon as a low-boiling point solvent is present in the formulation, for

instance diethyl ether (Celzard et al., 2013), pentane (Celzard et al., 2015) or a mixture of both (Li et al., 2013).

Herein, tannin extract and furfuryl alcohol were first dissolved in water by mechanical stirring, and then formaldehyde (37% in water) and diethyl ether were added. After homogenisation of the mixture, the resultant viscous resin was poured into a cylindrical container of diameter 63 mm and height 103 mm. Then, para-toluenesulphonic acid (pTSA, 65% in water) was introduced and the blend was intimately mixed again for a few seconds. pTSA catalysed the very exothermic polymerisation reactions, so that diethyl ether started to boil, and hence to produce a dramatic expansion of the material. At the same time, the heat that was generated helped hardening the as-produced foam so that it never collapsed and continued growing from the surface of the still liquid resin. Table 1 gathers the nature, the role and the amount of each ingredient used in the formulation.

2.2. Investigation methods

An experimental setup was specially designed for the present work, enabling the continuous measurements of temperature, deformation and mass (Figure 1). The temperature was recorded at three different positions of the foam during its different steps of growth, stabilisation/hardening and cooling. Two K-type thermocouples were installed at fixed points, one being located at 1.2 cm from the bottom of an HDPE beaker in which the foam was grown, and the other at 6 cm from the bottom. For avoiding as much as possible any disturbance of the foam rise due to the presence of these thermocouples, the latter were introduced from below into the beaker, through well-adjusted pinholes, and oriented along its revolution axis. The beaker was itself installed on a heavy wooden support throughout which the thermocouples were inserted. The whole was installed on an electronic balance (ENTRIS623I-1S 620G X) with resolution of 0.001 g. Thanks to this special design, the wires

of the thermocouples produced a negligible friction on the rising foam and did not interfere either with the weight measurements (Figure 2a).

The third measurement point was the upper surface of the foam, whose temperature was monitored using an infrared camera (OPTRIS PI 640 O33 T900) placed above the balance with a tripod (**Figure 1**b).

A camera (Logitech C925 1920x1080 Webcam Full HD Webcam) was also placed just in front of the electronic balance, at beaker level. After processing, the images were binarised so that the material appeared black and the background appeared white, as clearly shown in Figure 2b. Based on such binarised images, the projected area of the foam at every moment could be accurately determined. Then, a relative area was determined by calculating the ratio of the foam projected area at each time step ($t > 0$) to its initial area ($t = 0$). Finally, the mass of the foam was measured as a function of time thanks to the aforementioned balance connected to an acquisition unit.

The webcam and the balance were connected to a computer. The thermocouples were plugged into a NI 9211 thermocouple input module, itself connected to the same computer through a cDAQ-9174 chassis. The triggering of the recording and the acquisition were simultaneously carried out by the LabView software at a frequency of 3 measurements per second. During the expansion of the foam, the top of the foam cracked, letting appear part of the still hot material beneath the surface, which therefore was not representative of the actual surface temperature. The relevant zone for evaluating the correct temperature of the top surface of the foam was then chosen as a large crack-free area identified after viewing the video from the infrared camera (see "Area" in Figure 3).

3 Results and discussion

The results concerning the "standard" formulation are first given below. Then, the effects of changing the amounts of diethyl ether on the one hand, and of pTSA on the other hand, are discussed.

3.1 Studies of the standard formulation

3.1.1 Temperature variation as a function of time

As explained in the previous section, the temperatures were measured at three different positions: at the top surface with the infrared camera (here referred to as "Top"), and at two fixed positions with thermocouples at 1.2 cm and 6 cm from the bottom of the beaker (here referred to as "Bottom" and "Middle", respectively). Generally speaking, these 3 temperatures changed with time as described below.

A first stage was observed with a rapid increase of temperature during the first seconds of the experiment, until a maximum was reached after around 60 s. Then, cooling was observed until the return to the outside temperature (Figure 4a). The stage of temperature rise is obviously due to the exothermic polymerisation reactions occurring in the resin, since the very same process is exploited for producing the foam, as already detailed in subsection 2.1. Once these reactions are completed, the only remaining phenomenon is the convective and radiative heat exchange with the atmosphere, which induces the cooling of the material. At the maximum of temperature, it can be seen that “middle” temperature is the highest, followed by “bottom” and finally “top” temperature. As “bottom” and “top” temperatures are measured near the surface, they are submitted to a higher cooling heat flux than in the “middle” of the foam, because the atmosphere temperature was close to 20°C. If the “bottom” of the foam had been insulated, the temperature measured there would have been the highest, followed by the "middle" temperature, and the "top" temperature would have been the lowest.

Regarding the bottom probe, the first recorded temperature was 30°C because the reaction already started before the resin was completely poured into the beaker, 30 s of mixing being necessary after the addition of the catalyst (pTSA). As clearly shown in Figure 4b, the increase of temperature is not linear. Acceleration can be observed between 0 and 35 s, followed first by a pseudo-plateau until 50 s at a temperature close to 55 °C and then by another fast increase until the temperature saturates at its maximum value.

The plateau observed at 55°C was confirmed by plotting the derivative of the temperature with respect to time as a function of temperature (Figure 5), evidencing two inflection points and, between them, a minimum corresponding to the intermediary plateau. This finding suggests that some phenomenon absorbs energy, offsets the exothermic reaction, and hence delays and reduces the increase of temperature.

The temperature in the middle of the foam increased sharply because of the fixed position of the sensor which was not in contact with the material at the beginning of the measurements (see again Figure 4). Once the foam expanded enough (within 30 s), it touched the thermocouple, thus explaining the sudden rise of temperature. Once buried inside the foam, the middle probe logically experienced the highest temperature (about 90°C).

Interestingly, this maximum is synchronised in time (about 60 s, see Figure 4a) with that of the bottom temperature. Moreover, the decrease of temperature beyond the maximum followed the same regime for both bottom and middle points (Figure 4a), which suggests that heat exchanges (both radiative and convective) with the exterior prevail. Here, no phase change such as condensation of diethyl ether vapours was observed.

The way the surface temperature changed with time was different from that of the two other positions. Not only the maximum was reached faster, i.e., at shorter time than the others (see again Figure 4b), but the temperature also dropped quite fast and reached values as low as 16°C, i.e., below room temperature (which was 20°C during all the experiments). The latter

finding is clearly seen on the infrared picture at 858 s, see Figure 6. It is likely that the different behaviour of the surface temperature is due to the evaporation of the blowing agent (diethyl ether), which necessarily occurs at the surface of the material. Such evaporation was confirmed by the continuous mass loss observed in Figure 8 (see below). Evaporation is a phase change and therefore induces a significant absorption of heat, leading to the faster decrease of the surface temperature. As the latter is in thermal equilibrium with ambient air, the heat extraction related to evaporation imposes a temperature lower than that of the atmosphere.

By observing the images of the infrared camera (Figure 6), it can be seen that, within a range of a few seconds, the surface temperature is rather homogeneous from one area to another, except where cracks appeared on the skin of the foam. These images support that the area selected in Figure 3 was relevant for describing the overall behaviour of the surface temperature.

3.1.2 Expansion as a function of time

As explained in subsection 2.1, the relative changes of volume were not directly measured, but are expected to be proportional to the changes of projected area determined after binarisation of the foam images caught by the webcam (Figure 2b). Foam expansion occurred in three distinct phases, see Figure 7, and especially Figure 7b. In the first phase, i.e., at the very beginning of the foaming process, the volume remained constant for 25 s. The expansion could indeed not start as long as diethyl ether did not reach its phase change temperature (34°C if pure). After such induction time, diethyl ether turned from liquid to vapour and hence expansion occurred. The production of vapour, along with the increase of temperature, creates a mechanical balance between the inner pressure (within the pores) and the skin of the material. As the polymer matrix is poorly viscous at the beginning of the process, the inner

pressure prevails and outweighs the surface energy, and hence the volume increases. The observed expansion lasted for about 20 s.

Figure 7c shows the change of relative expansion as a function of bottom temperature, and its corresponding derivative. The bottom temperature was chosen instead of that of the middle because the thermocouple is continuously immersed in the mixture. Unlike what was conjectured above, the expansion did not only occur at 34°C. While the phenomenon indeed (slowly) began at the expected phase change temperature of pure diethyl ether, it continued in a range of higher temperatures and was even the fastest at 55°C. It is quite possible that blending diethyl ether with other solutes (water solutions of formaldehyde and pTSA, both present in the formulation, as well as impurities coming from the tannin extract and dissolved in water, such as alkali) produced an increase of boiling point, which is a classic colligative property that one may expect (Raoult's law). Moreover, the highest expansion rate occurring at 55°C coincides with the pseudo-plateau of bottom temperature already observed in Figure 4b, and therefore further supports the assumption of phase change of a mixture of diethyl ether and aqueous solution instead of pure blowing agent.

The end of the expansion can be explained by two simultaneous phenomena. The first one corresponds to the hardening of the polymer matrix, which prevents any further deformation after a given time controlled by the polymerisation kinetics. The second phenomenon is related to the opening of the porosity by rupture of cell walls, resulting in a balance between internal and ambient pressures and thus stopping the expansion (see below the discussion about weight loss). Finally, a very low shrinkage can be observed at high time in Figure 7b, due to both cooling and to the relatively fast expansion rate but low crosslinking rate of the polymer matrix.

3.1.3 Mass variation as a function of time

The relative changes of mass are shown in Figure 8, and three successive steps can be observed over time. The first one is a linear but very low mass decrease during the first 25 s of the experiment. Then, a sudden and exponential decrease of mass occurs. Finally, a slow and roughly linear mass loss is seen, expected to tend towards a constant value after quite a long time. The transition between 1st and 2nd steps corresponds to the onset of foam expansion, while that between 2nd and 3rd steps seems to be related to the moment at which both bottom and middle temperatures start to decrease, as seen in Figure 4b. Such moment coincides with the depletion of the reagents present in the system. The observed phenomena can be detailed further and are discussed as follows.

In step 1, the mass loss is very low and most probably corresponds to the surface evaporation of the liquid resin, driven by the difference of vapour pressure of either diethyl ether or water, or both, between the material surface and the atmosphere. For instance, since water is in liquid phase before foaming, the surface can be considered as saturated and, at 20°C, the saturation pressure is equal to 2300 Pa. If in the atmosphere, the relative humidity is 50% and the temperature is again 20°C, the vapour pressure becomes equal to 1150 Pa, and therefore evaporation mass flow should exist at the surface of the resin. The evaporation mass flow, F_m (kg s^{-1}), indeed reads:

$$F_m = -\int_0^S k_m \frac{M_v}{R}\left(\frac{p_{v;a}}{T_a} - \frac{p_v}{T}\right) dS \qquad (1)$$

where k_m (m s^{-1}) is the convective mass transfer coefficient, S (m^2) is the exchange area, T_a and T (K) are the temperatures of air and material surface, respectively, P_{va} and P_v (Pa) are the vapour pressures in air and at the surface of the material, respectively, M_v (kg mol^{-1}) is the molecular weight of the vapour, and R (J mol^{-1} K^{-1}) is the ideal gas constant. Thus, taking into account the aforementioned values of saturation pressure and vapour pressure, the

difference of p_v/T ratios in Eq. (1) between the atmosphere and the surface becomes positive (3.92 Pa K^{-1}), which indeed induces a negative mass flux and therefore a loss of mass.

This assumption also applies to diethyl ether as well as to any other volatile constituent of the formulation, such as formaldehyde. The amount of diethyl ether in the beaker induces a vapour pressure at the surface of the liquid resin, which is always higher than the vapour pressure in air, assumed to be close to zero.

The 2nd step, corresponding to a steep loss of mass of a few %, occurred during the expansion of the material. It was observed that the foam, once stabilised, contains open porosity. The transition from closed to open porosity allows explaining such abrupt mass loss. Indeed, during foam growth, the total pressure which is generated, and which is initially trapped as bubbles in the viscous resin, increases with the amount of diethyl ether undergoing phase change from liquid state to vapour. After a critical volume increase, pore opening occurs, driven by the difference of pressure between the core of the foam and the atmosphere, and thus creating a continuity of the gas phase with the exterior. Darcy's law may explain gas transfers in a porous matrix submitted to a pressure gradient, established at the moment at which the pores open: it states that the gas velocity, v (m s^{-1}), is proportional to the pressure gradient and to the permeability of the medium, according to:

$$\vec{v} = -\frac{k}{\mu}\vec{\nabla}P \qquad (2)$$

where k (m^2) is the gas permeability of the foam, μ (Pa s) is the gas dynamic viscosity, and ∇P (Pa) is the gas pressure gradient.

Thus, the pressure gradient produced at the onset of pore opening leads to a sudden flow of gas expelled from the material. For instance, if an (arbitrarily chosen but still realistic) overpressure of 1000 Pa is considered between the core of the material and its upper surface,

let $P\ (x = 0) = 1000 + P_{atm}$ and $P\ (x = L) = P_{atm}$, where L is the distance between the middle part of the foam and its upper surface (average of 7.5 cm) and P_{atm} is the atmospheric pressure. Thus, the pressure gradient is -1000 / 0.075 = -13333.3 Pa m^{-1}. Considering a gas permeability of 10^{-11} m^2 and a viscosity of 0.224 mPa s, a speed of 5.95 10^{-4} m s^{-1} is calculated. This calculated flux is positive, so a transfer of gas to the exterior can indeed exist.

This phenomenon can be observed with the infrared camera during the expansion of the foam, as shown in Figure 9. A flux of gas expelled from the foam and hotter than the surrounding atmosphere is indeed clearly seen in Figure 9b.

Finally, the last step of mass loss is slow and rather constant with time. Indeed, once the total pressures inside and outside the foam are balanced, Darcy's flow vanishes, which marks the end of the previous rapid mass loss (step #2). Observing the fresh foam reveals that its porous structure is wet, and the final mass loss step thus corresponds to drying. The surface evaporation observed here is explained by the same phenomenon as in step #1, i.e., by a difference of vapour pressure between the material surface and the atmosphere. Another hint that can explain this phenomenon is related to the temperature at the surface. Indeed, it was observed that the latter was lower than the external temperature at the end of the experiment (see again Figure 4a). This is a very usual finding when it comes to drying in air, because the energy required to evaporate the liquid decreases the temperature of the wet material surface.

3.2 Impact of the amount of diethyl ether

The previous section was dedicated to foaming studies of the standard formulation described in Table 1, i.e., using 3g of diethyl ether. Herein, the same formulation was investigated but using two different amounts of blowing agent: 1g or 5g of diethyl ether. Figure 10 clearly shows the dramatic impact of this ingredient on the expansion of the foam, already demonstrated (Celzard et al., 2010, 2012, 2015; Li et al., 2013; Tondi et al., 2009b)

and quantitatively established (Amaral-Labat et al., 2013; Letellier et al., 2017b, 2017a; Li et al., 2012b; Zhao et al., 2010) in former works from our group.

The curves presented in Figure 11a, 11b, 11c and 11d show that the lower was the amount of blowing agent, the higher was the maximum temperature obtained and the faster it was reached. This finding is readily explained by considering the sensible heat transfer from the exothermic reaction to the diethyl ether: more energy must indeed be brought for increasing the temperature of the liquid blowing agent until it reaches its phase change temperature, thus slowing down the rise of the overall material temperature. But the phase change of a higher amount of diethyl ether also requires more energy, and such impact of the latent heat transfer can be seen in Figure 11b, showing a longer pseudo-plateau of temperature related to phase change, thereby delaying further the increase of overall temperature.

In contrast, a larger amount of blowing agent led to faster cooling. This phenomenon is not only explained by the correspondingly lower temperatures discussed above, since the change of temperature with time is faster. As the volume of the foam increases sharply with the amount of diethyl ether (see Figure 10 and 11e), the exchange surface area increases accordingly. And since the convective heat flux, ϕ_{cv} (W), increases with the exchange area (see Eq. (3)), it is thus logical to observe a faster temperature decrease:

$$\phi_{cv} = \int_0^S h\left(T_a - T\right) dS \tag{3}$$

In Eq. (3), h (W m^{-2} K^{-1}) is the convective heat transfer coefficient, S (m²) is the exchange area, and T_a and T (K) are the temperatures of air and material surface, respectively.

As expected, the relative deformation increased with the amount of diethyl ether (Figure 10 and 11e) since more liquid was converted into vapour. Regarding mass changes, the sudden loss of mass due to pore opening varied accordingly, so that higher mass losses were obtained

with more blowing agent in the formulation. The evaporation mass flow was also higher because, as suggested by Eq. (1), it depends on the exchange area with the exterior, which was higher with foams produced with more diethyl ether.

3.3 Impact of the amount of catalyst

The present section is now dedicated to the effect of the amount of polymerisation catalyst added to the standard formulation, using either 9 or 13g of pTSA, instead of 11g as formerly presented in Table 1. As a general trend, and whereas all changes remained qualitatively the same, decreasing the amount of pTSA delayed all phenomena, whether peak of temperature, expansion, or mass loss (Figure 12). The effect was rather low with respect to what was observed for the standard formulation when the amount of catalyst was increased, but the foam expansion took typically two times longer by using 9g of pTSA instead of 11. The latter finding is quite interesting in case one would like to delay the onset of foaming, for instance for having enough time for pouring the liquid formulation into a mould.

4 Conclusion

An experimental setup was designed for continuously measuring the temperature at different positions, the expansion, and the changes of mass of a phenolic/furanic foam all along its growth from a self-foaming, tannin-based biosourced formulation. New phenomena were observed:

- the energy absorbed by the phase change of the blowing agent (DEE) offset the exothermic reaction and limited the increase of temperature at the resin – growing foam interface;
- the expansion did not only occur at the phase change temperature of pure DEE (34°C), but took place in a range of higher temperatures and was even the fastest at 55°C;
- more blowing agent led to lower foaming temperature, explained by the enhanced latent heat transfer, and to higher evaporation-induced mass flow, explained by the larger exchange area, which also elucidated the faster cooling rate;

- more catalyst only accelerated the phenomena, which remained qualitatively the same.

The continuous measurement of mass loss, carried out for the first time in this context, revealed a succession of three phases:

- a short drying one before expansion, explained by liquid evaporation at the surface;
- a sudden loss of mass during expansion, corresponding to a steep loss of mass of a few % and observed with an infrared camera, induced by a pressure gradient driven by the onset of pore opening at a critical inner pressure;
- an ongoing evaporation until complete drying of the as-produced thermoset foam. A surface evaporation phenomenon was evidenced, resulting in a surface temperature that decreased fast until below the atmospheric temperature during cooling.

The new phenomena highlighted in this study should allow developing new ways of foam optimisation. Especially, the phenomenon of pore opening is crucial for the final quality of the material. As for the phenomenon of drying, poorly studied so far, it shows that the foam formation is not finished at the end of the expansion, but continues until final drying.

Acknowledgements

The authors gratefully acknowledge the financial support of the “Pôle M4” of University of Lorraine and FEDER funds through the TALiSMAN project. Engineering students Eva Dano and Michel Haubold are thanked for supplying the raw data from which the present work could be successfully carried out.

References

Amaral-Labat, G., Gourdon, E., Fierro, V., Pizzi, A., and Celzard, A. (2013). Acoustic properties of cellular vitreous carbon foams. Carbon *58*, 76–86.

Basso, M.C., Li, X., Fierro, V., Pizzi, A., and Celzard, A. (2011). Green, formaldehyde-free, foams for thermal insulation. Adv. Mater. Lett. *2*, 378-382M.

Basso, M.C., Giovando, S., Pizzi, A., Celzard, A., and Fierro, V. (2013a). Tannin/furanic foams without blowing agents and formaldehyde. Ind. Crops Prod. *49*, 17–22.

Basso, M.C., Pizzi, A., and Celzard, A. (2013b). Dynamic Monitoring of Tannin-based Foam Preparation: Effects of Surfactant. BioResources *8*, 5807-5816–5816.

Basso, M.C., Pizzi, A., and Celzard, A. (2013c). Influence of formulation on the dynamics of preparation of tannin-based foams. Ind. Crops Prod. *51*, 396–400.

Basso, M.C., Pizzi, A., and Celzard, A. (2013d). Dynamic Foaming Behaviour of Polyurethane vs Tannin/Furanic Foams. J. Renew. Mater. *1*, 273–278.

Basso, M.C., Giovando, S., Pizzi, A., Lagel, M.-C., and Celzard, A. (2014a). Alkaline Tannin Rigid Foams. J. Renew. Mater. *2*, 182–185.

Basso, M.C., Delmotte, L., Al-Marzouki, F., Abdalla, S., and Celzard, A. (2014b). MALDI-TOF and 13C NMR Analysis of Tannin–Furanic–Polyurethane Foams Adapted for Industrial Continuous Lines Application. Polymers *6*, 2985–3004.

Basso, M.C., Lagel, M.-C., Pizzi, A., Celzard, A., and Abdalla, S. (2015). First Tools for Tannin-Furanic Foams Design. BioResources *10*.

Bikard, J., Bruchon, J., Coupez, T., and Vergnes, B. (2005). Numerical prediction of the foam structure of polymeric materials by direct 3D simulation of their expansion by chemical reaction based on a multidomain method. J. Mater. Sci. *40*, 5875–5881.

Bikard, J., Bruchon, J., Coupez, T., and Silva, L. (2007). Numerical simulation of 3D polyurethane expansion during manufacturing process. Colloids Surf. Physicochem. Eng. Asp. *309*, 49–63.

Bo, C., Wei, S., Hu, L., Jia, P., Liang, B., Zhou, J., and Zhou, Y. (2016). Synthesis of a cardanol-based phosphorus-containing polyurethane prepolymer and its application in phenolic foams. RSC Adv. *6*, 62999–63005.

Bo, C., Hu, L., Chen, Y., Yang, X., Zhang, M., and Zhou, Y. (2018). Synthesis of a novel cardanol-based compound and environmentally sustainable production of phenolic foam. J. Mater. Sci. *53*, 10784–10797.

Bouayad, R., Bikard, J., and Agassant, J.F. (2008). Injection of thermoset foam: comparison between simulation and experiment. Int. J. Mater. Form. *1*, 683–686.

Bouayad, R., Bikard, J., and Agassant, J.-F. (2009). Compressible flow in a plate/plate rheometer: application to the experimental determination of reactive expansion's models parameters for polyurethane foam. Int. J. Mater. Form. *2*, 243.

Braghiroli, F.L., Fierro, V., Izquierdo, M.T., Parmentier, J., Pizzi, A., and Celzard, A. (2012). Nitrogen-doped carbon materials produced from hydrothermally treated tannin. Carbon *50*, 5411–5420.

Carvalho, G. de, Pimenta, J.A., Santos, W.N. dos, and Frollini, E. (2003). Phenolic and Lignophenolic Closed Cells Foams: Thermal Conductivity and Other Properties. Polym.-Plast. Technol. Eng. *42*, 605–626.

Celzard, A., Zhao, W., Pizzi, A., and Fierro, V. (2010). Mechanical properties of tannin-based rigid foams undergoing compression. Mater. Sci. Eng. A *527*, 4438–4446.

Celzard, A., Tondi, G., Lacroix, D., Jeandel, G., Monod, B., Fierro, V., and Pizzi, A. (2012). Radiative properties of tannin-based, glasslike, carbon foams. Carbon *50*, 4102–4113.

Celzard, A., Fierro, V., Pizzi, A., and Zhao, W. (2013). Multifunctional porous solids derived from tannins. J. Phys. Conf. Ser. *416*, 012023.

Celzard, A., Szczurek, A., Jana, P., Fierro, V., Basso, M.-C., Bourbigot, S., Stauber, M., and Pizzi, A. (2015). Latest progresses in the preparation of tannin-based cellular solids. J. Cell. Plast. *51*, 89–102.

Delgado-Sánchez, C., Sarazin, J., Santiago-Medina, F.J., Fierro, V., Pizzi, A., Bourbigot, S., and Celzard, A. (2018a). Impact of the formulation of biosourced phenolic foams on their fire properties. Polym. Degrad. Stab. *153*, 1–14.

Delgado-Sánchez, C., Santiago-Medina, F., Fierro, V., Pizzi, A., and Celzard, A. (2018b). Optimisation of "green" tannin-furanic foams for thermal insulation by experimental design. Mater. Des. *139*, 7–15.

Denslow, K.R., and Rickle, G.K. (1989). Surfactant Effects in Phenolic Foam Resins. J. Cell. Plast. *25*, 31–42.

Haberstroh, E., and Schlumm, M. (2011). Properties and Manufacturing of Sandwich Parts with Phenolic Foam Cores. J. Polym. Eng. *26*, 213–226.

Ireka, I.E., Niedziela, D., Schäfer, K., Tröltzsch, J., Steiner, K., Helbig, F., Chinyoka, T., and Kroll, L. (2015). Computational modelling of the complex dynamics of chemically blown polyurethane foam. Phys. Fluids 1994-Present *27*, 113102.

Karimi, M., and Marchisio, D.L. (2015). A Baseline Model for the Simulation of Polyurethane Foams via the Population Balance Equation: A Baseline Model for the Simulation of Polyurethane…. Macromol. Theory Simul. *24*, 291–300.

Lacoste, C., Basso, M.C., Pizzi, A., Laborie, M.-P., Celzard, A., and Fierro, V. (2013). Pine tannin-based rigid foams: Mechanical and thermal properties. Ind. Crops Prod. *43*, 245–250.

Lacoste, C., Pizzi, A., Basso, M.-C., Laborie, M.-P., and Celzard, A. (2014). Pinus pinaster tannin/furanic foams: PART I. Formulation. Ind. Crops Prod. *52*, 450–456.

Lagel, M.-C., Pizzi, A., Giovando, S., and Celzard, A. (2014). Development and Characterisation of Phenolic Foams with Phenol-Formaldehyde-Chestnut Tannins Resin. J. Renew. Mater. *2*, 220–229.

Landrock, A.H. (1995). Handbook of Plastic Foams: Types, Properties, Manufacture and Applications (Noyes Publications, Park Ridge, New Jersey, USA).

Letellier, M., Szczurek, A., Basso, M.-C., Pizzi, A., Fierro, V., Ferry, O., and Celzard, A. (2017a). Preparation and structural characterisation of model cellular vitreous carbon foams. Carbon *112*, 208–218.

Letellier, M., Macutkevic, J., Bychanok, D., Kuzhir, P., Delgado-Sanchez, C., Naguib, H., Mosanenzadeh, S.G., Fierro, V., and Celzard, A. (2017b). Modelling the physical properties of glasslike carbon foams. J. Phys. Conf. Ser. *879*, 012014.

Li, X., Basso, M.C., Fierro, V., Pizzi, A., and Celzard, A. (2012a). Chemical modification of tannin/furanic rigid foams by isocyanates and polyurethanes. Maderas Cienc. Tecnol. *14*, 257–265.

Li, X., Basso, M.C., Braghiroli, F.L., Fierro, V., Pizzi, A., and Celzard, A. (2012b). Tailoring the structure of cellular vitreous carbon foams. Carbon *50*, 2026–2036.

Li, X., Pizzi, A., Lacoste, C., Fierro, V., and Celzard, A. (2013). Physical Properties of Tannin/Furanic Resin Foamed With Different Blowing Agents. BioResources *8*, 743-752–752.

Marie, Z., Nicolas, V., Celzard, A., and Fierro, V. (2019). First approach for modelling the physical foaming of tannin-based thermoset foams. Int. J. Therm. Sci. *(submitted to)*.

Martinez de Yuso, A., Lagel, M.C., Pizzi, A., Fierro, V., and Celzard, A. (2014). Structure and properties of rigid foams derived from quebracho tannin. Mater. Des. *63*, 208–212.

Mendelsohn, M.A., Meier, J.F., Rudd, G.E., and Rosenblatt, G.B. (1979a). Effects of density and structure on load bearing and permeability characteristics of a family of shock mitigating phenolic foams. J. Appl. Polym. Sci. *23*, 333–339.

Mendelsohn, M.A., Meier, J.F., Rudd, G.E., and Rosenblatt, G.B. (1979b). Effects of composition and processing conditions on the properties of a series of shock mitigating phenolic foams. J. Appl. Polym. Sci. *23*, 341–351.

Pizzi, A., Tondi, G., Pasch, H., and Celzard, A. (2008). Matrix-assisted laser desorption/ionization time-of-flight structure determination of complex thermoset networks: Polyflavonoid tannin–furanic rigid foams. J. Appl. Polym. Sci. *110*, 1451–1456.

Rangari, V.K., Hassan, T.A., Zhou, Y., Mahfuz, H., Jeelani, S., and Prorok, B.C. (2007). Cloisite clay-infused phenolic foam nanocomposites. J. Appl. Polym. Sci. *103*, 308–314.

Shen, H., and Nutt, S. (2003). Mechanical characterization of short fiber reinforced phenolic foam. Compos. Part Appl. Sci. Manuf. *34*, 899–906.

Shutov, F.A. (1984). Phenolic foams in the USSR. Cell. Polym. *3*, 95–104.

Tondi, G., Zhao, W., Pizzi, A., Du, G., Fierro, V., and Celzard, A. (2009a). Tannin-based rigid foams: a survey of chemical and physical properties. Bioresour. Technol. *100*, 5162–5169.

Tondi, G., Blacher, S., Léonard, A., Pizzi, A., Fierro, V., Leban, J.M., and Celzard, A. (2009b). X-Ray Microtomography Studies of Tannin-Derived Organic and Carbon Foams. Microsc. Microanal. *15*, 384–394.

Zhao, W., Pizzi, A., Fierro, V., Du, G., and Celzard, A. (2010). Effect of composition and processing parameters on the characteristics of tannin-based rigid foams. Part I: Cell structure. Mater. Chem. Phys. *122*, 175–182.

499

500 **Table 1:** Standard formulation of tannin-based foam

Ingredients and roles in the formulation	Mass (g)
Mimosa tannin extract; base of the resin	30
para-toluenesulphonic acid (pTSA, 65% in water); catalyst	11
Furfuryl alcohol; co-reagent producing heat upon polymerisation	10.5
Formaldehyde (37% in water); crosslinker	7.4
Water; solvent	6
Diethyl ether (DEE); (physical) blowing agent	3

501

502

Figure caption

Figure 1: Specially designed system for the continuous and simultaneous measurements of foam temperature, deformation and mass during growth, hardening and cooling: (a) schematic view; (b) actual system installed in a fume hood.

Figure 2: (a) Zoom of the thermocouples passing through the beaker via a wooden support placed on an electronic balance, and whose probes are located at two different positions from the bottom; (b) real image of the foam caught by camera after growth, and its binarised counterpart used to calculate the foam's relative area as a function of time.

Figure 3: Infrared image showing the area chosen for measuring the surface temperature.

Figure 4: Variation of temperature with time at three positions of the foam: bottom (green continuous line), middle (red dashed line), top (blue dotted line): (a) whole curves; and (b) zoom on the first 100 s.

Figure 5: Time derivative of the bottom temperature, as a function of temperature.

Figure 6: Infrared pictures of the growing foam as a function of time. The colour bar corresponds to a temperature range from 16°C to 55°C.

Figure 7: Relative deformation of the foam as a function of time: (a) whole curve; (b) zoom on the first 100 s; (c) Same as (b) but as a function of bottom temperature, and corresponding derivative.

Figure 8: Relative mass change of the foam as a function of time.

Figure 9: Infrared pictures of the growing foam at two different times. The scale bar corresponds to a temperature range from 16°C to 30°C, and is given in black and white instead of colours as in Figure 6 for a better contrast.

Figure 10: Final morphology and volume of standard tannin-based foams produced with increasing amounts of blowing agent; from left to right: 1, 3 and 5 g of diethyl ether.

Figure 11: Data related to foaming of standard formulations prepared with three amounts of blowing agent (green: 1g of diethyl ether; red: 3g; and blue: 5g): (a) temperature changes at three positions within the foam (continuous lines: bottom; dashed lines: middle; dotted lines: top), and zooms on: (b) bottom, (c) top and (d) middle positions; (e) Relative deformation as a function of time; (f) Relative mass loss as a function of time.

Figure 12: Data related to foaming of standard formulations prepared with three amounts of catalyst (green: 9g of pTSA; red: 11g; and blue: 13g): (a) temperature changes at three positions within the foam (continuous lines: bottom; dashed lines: middle; dotted lines: top); and (b) zoom on the first 100 s; (c) Relative deformation as a function of time; (d) Relative mass loss as a function of time.

538

539 **Figure 1**

540

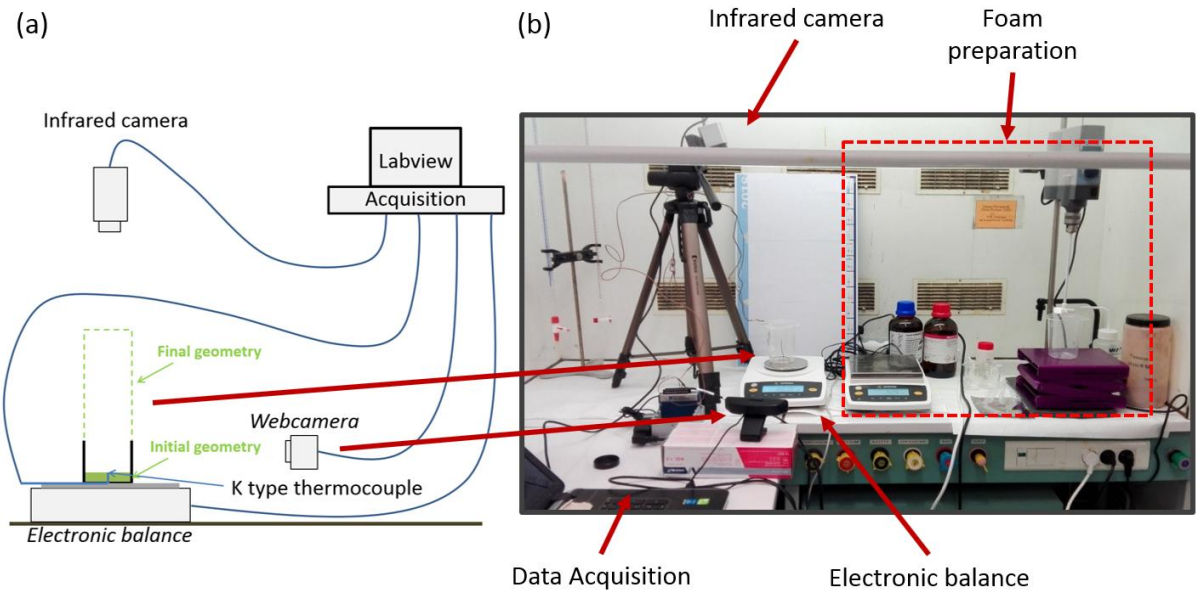

541

542
543

544

545 **Figure 2**

546

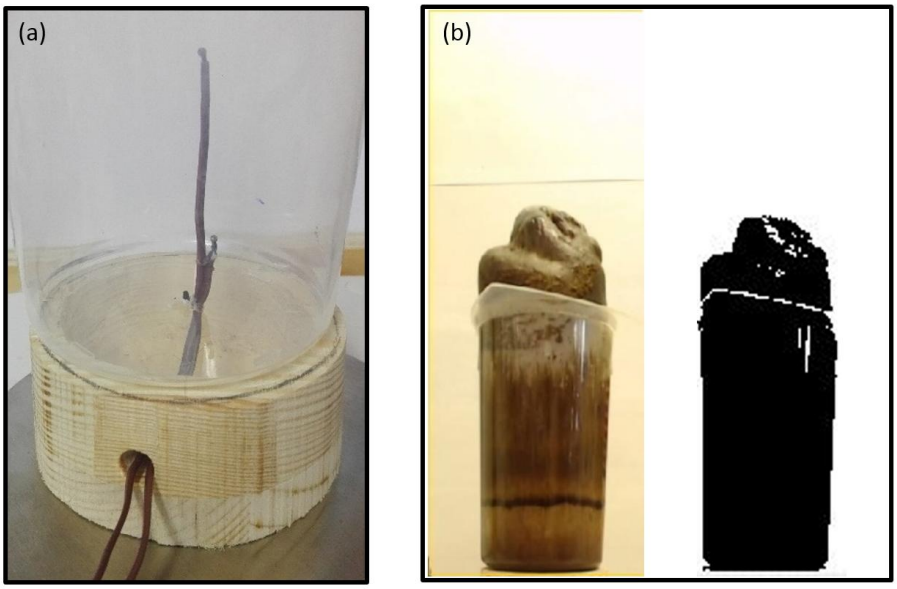

547

548

549

550

551

552 **Figure 3**

553

554

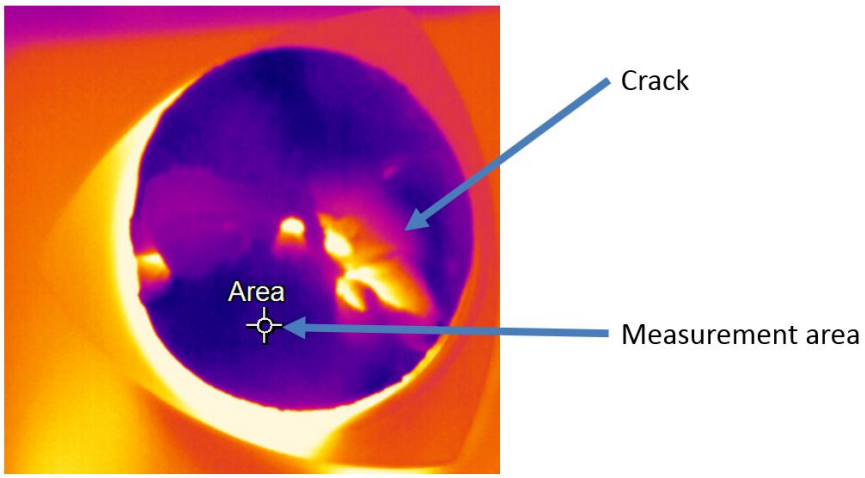

555

556

557

558

559

560 **Figure 4**

561

562

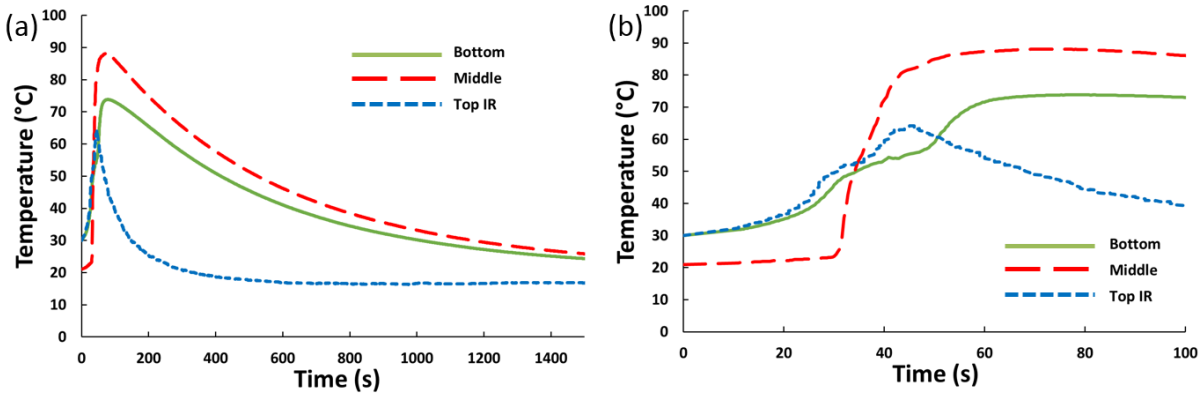

563

564

565

Figure 5

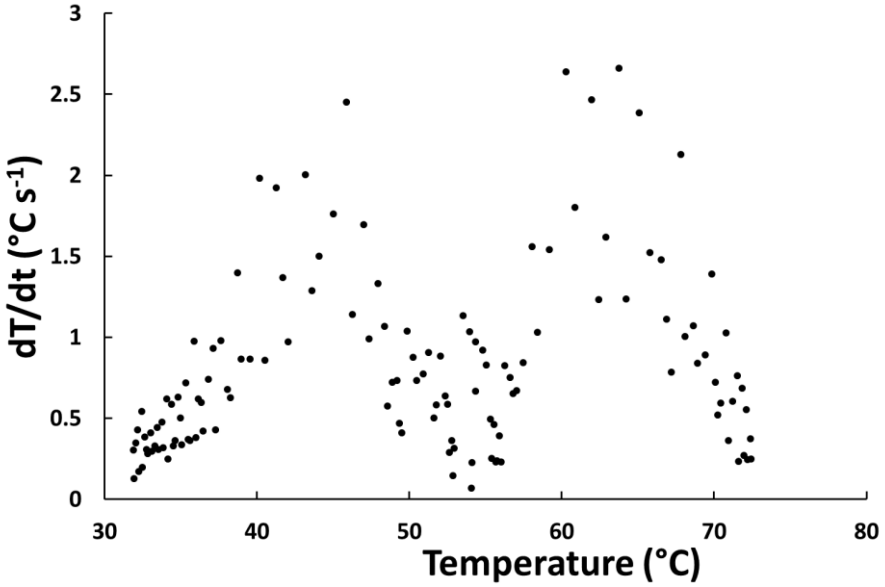

Figure 6

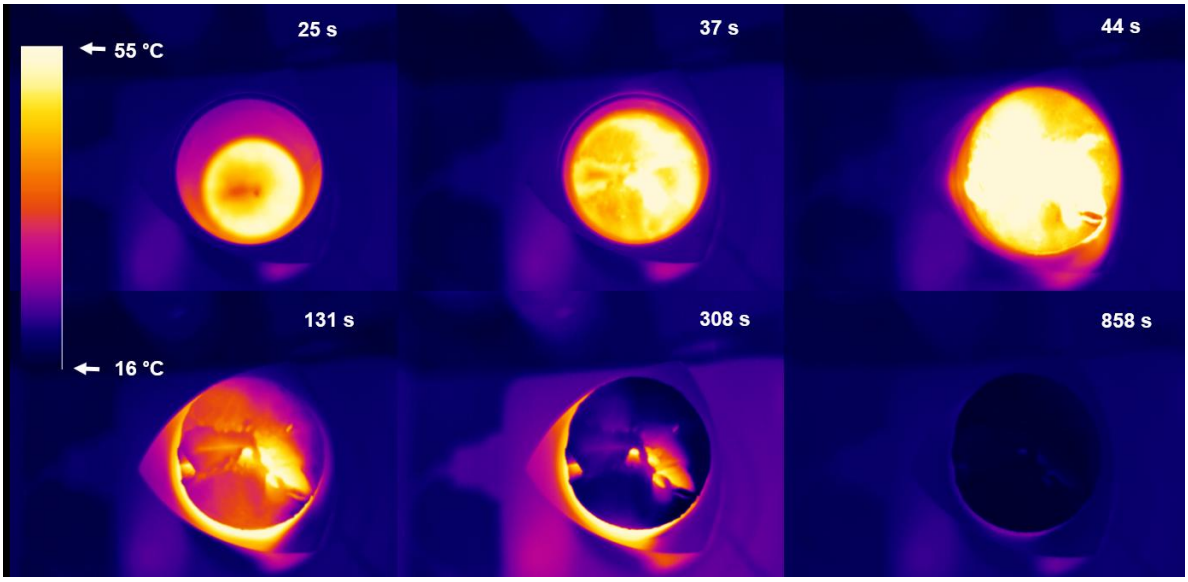

582

583 **Figure 7**

584

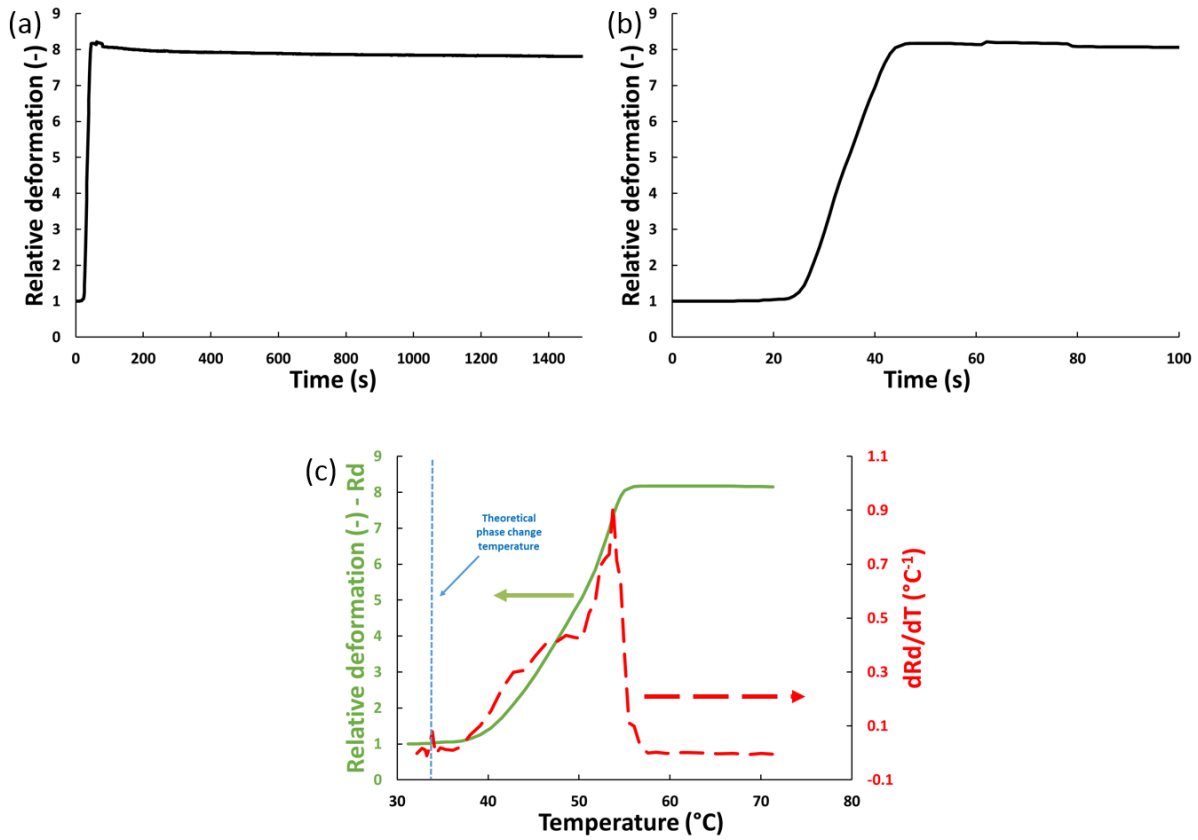

585

586

587

588

589 **Figure 8**

590

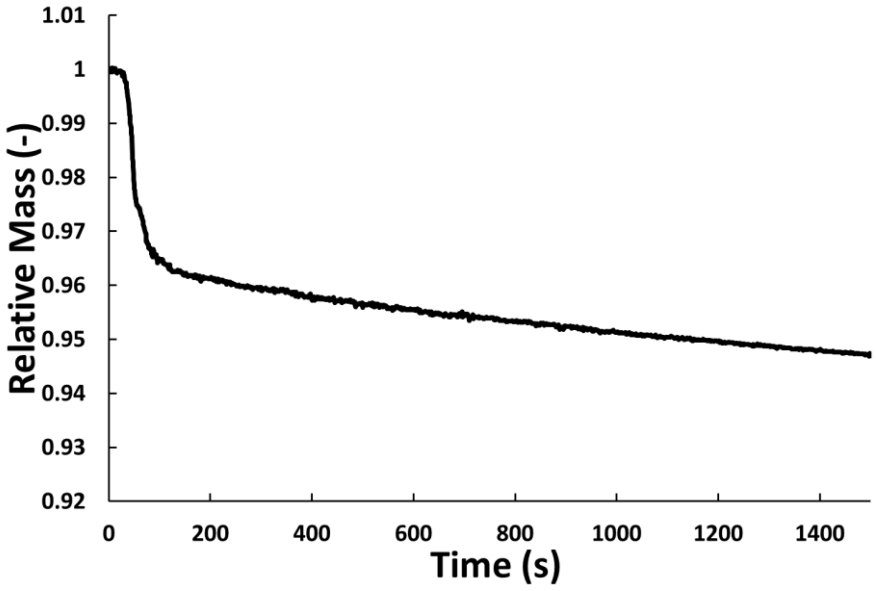

591

592

593

594

595

596

597 **Figure 9**

598

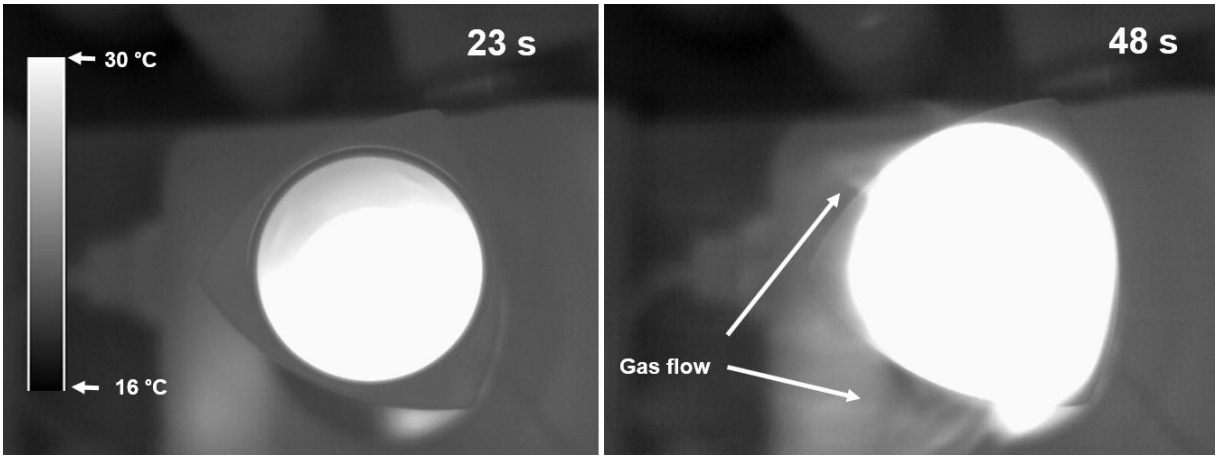

599

600

601

602

603

604

605 **Figure 10**

606

607

608

609

610

611

612 **Figure 11**

613

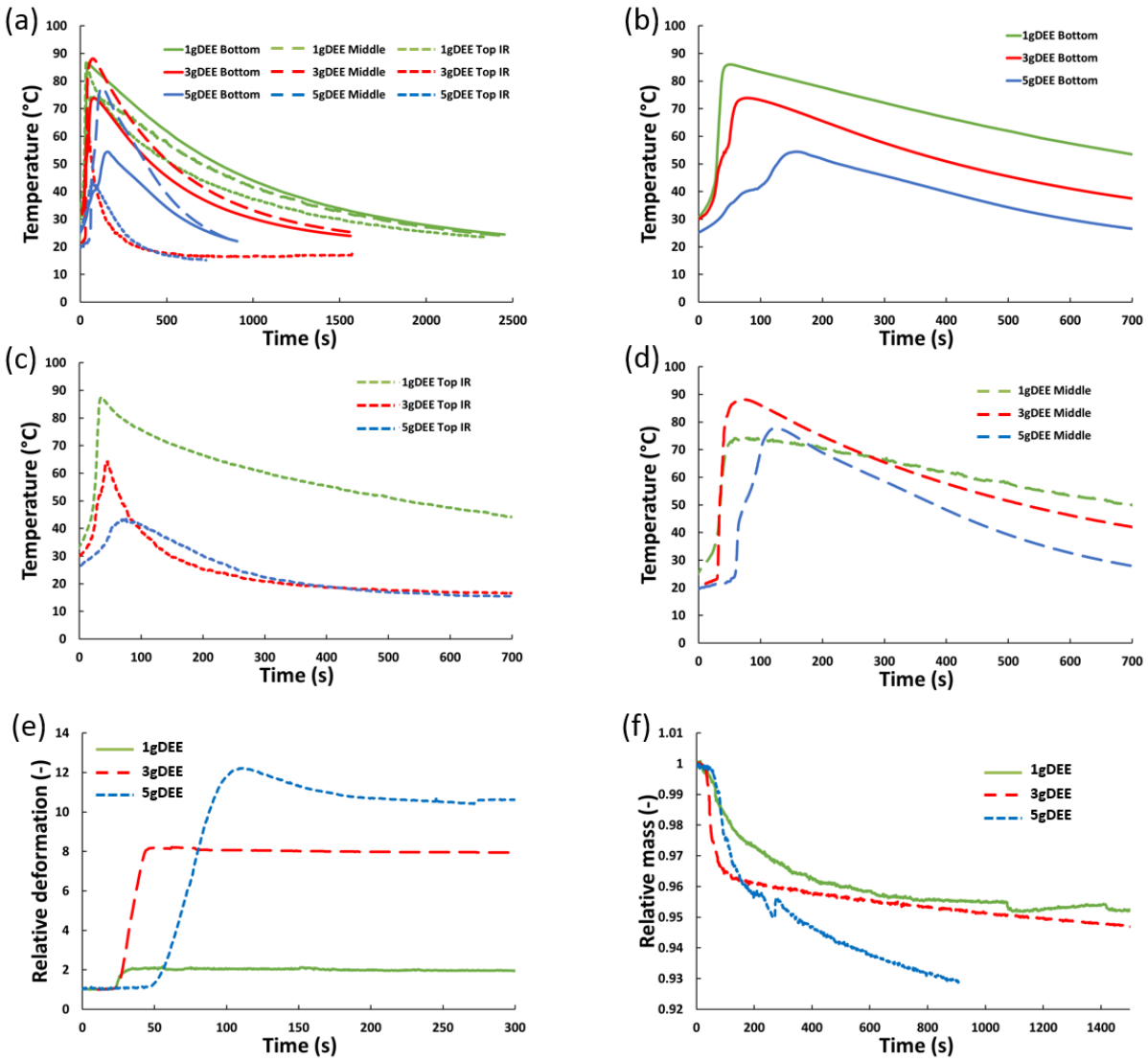

614

615

616

617

618

Figure 12

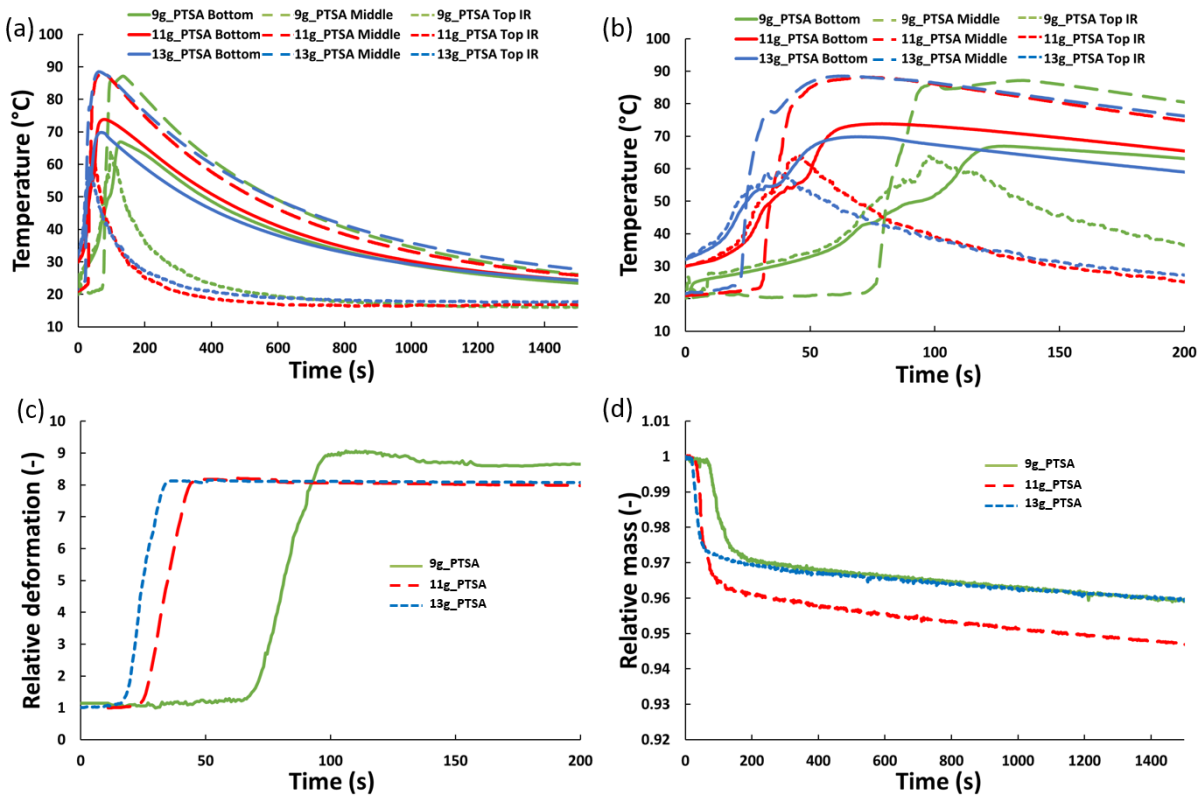
(a)
9g_PTSA Bottom
9g_PTSA Middle
9g_PTSA Top IR
11g_PTSA Bottom
11g_PTSA Middle
11g_PTSA Top IR
13g_PTSA Bottom
13g_PTSA Middle
13g_PTSA Top IR
Temperature (°C)
Time (s)
(b)
Temperature (°C)
Time (s)
(c)
Relative deformation (-)
9g_PTSA
11g_PTSA
13g_PTSA
Time (s)
(d)
Relative mass (-)
9g_PTSA
11g_PTSA
13g_PTSA
Time (s)